CONVERSION-ELECTRON MOSSBAUER SPECTROSCOPY OF AMORPHOUS IRON-GADOLINIUM THIN FILMS.

by

Peter Hargraves

A thesis
presented to the University of Manitoba
in partial fulfillment of the
requirements for the degree of
Master of Science
in
Department of Physics

Winnipeg, Manitoba, 1983

CONVERSION-ELECTRON MOSSBAUER SPECTROSCOPY OF AMORPHOUS IRON-GADOLINIUM THIN FILMS

BY

PETER HARGRAVES

A thesis submitted to the Faculty of Graduate Studies of the University of Manitoba in partial fulfillment of the requirements of the degree of

MASTER OF SCIENCE

ABSTRACT

Fe-Gd amorphous thin films, prepared by thermal evaporation in a vacuum were studied here using Conversion-Electron Mossbauer Spectroscopy (CEMS). The spectra obtained are representative of the surface (the first 1000 A) of the films. Also, depth selective spectra were obtained by selective voltage discrimination of the signal pulses as first described by Nakagawa (1982) et al . Depth selection was also attempted by evaporating a 2000 A layer of aluminum onto the surface in the same manner as Tricker et al (1979).

In addition two films were annealed at successively higher temperatures with CEMS used to ascertain the identity of the various phases present at each stage.

ACKNOWLEGEMENTS

I would like to thank Dr A.H. Morrish for his supervision of this project and for his encouragement. I am indebted to Dr. R.J. Pollard and Dr. N. Saegusa for their daily help and encouragement. Dr. Pollard is also to be thanked for making his extensive software available to me. Also I must thank Dr R.F. Soohoo of UC Davis for the annealing of my samples and Dr. R.C.Taylor of IBM for their fabrication. Finally, thanks are due to those Faculty members, graduate students and technical staff who kindly gave their help and advice to me during the course of this project.

CONTENTS

CHAPTER ONE: INTRODUCTION

1.1 MÖSSBAUER SPECTROSCOPY

The emission of a gamma ray from a free nucleus must obey the laws of conservation of energy and momentum. Therefore the nucleus recoils with the same momentum that the emitted gamma-ray possesses. It follows that the gamma ray will not possess the entire energy of the decay since some was imparted to the nucleus.If the nucleus is bound to the lattice of a solid it cannot recoil freely and two events are possible: firstly the recoil energy can be transferred to the vibrational modes of the lattice, or alternatively the whole lattice can recoil. (We ignore the case where the recoil energy is greater than the binding energy of the nucleus since this case is not of interest here).Since the vibrational energy levels of a solid are quantized, only certain discrete energies can be transferred to these vibrational modes and for recoil energies substantially different from these (or combinations of these) no such transfer will result. In this case the entire lattice will recoil. When this occurs the energy of recoil:

$$E^2/2Mc^2$$

where M is the lattice mass, E is the energy of the photon and c is the speed of light, will be reduced to an insignificant value since the mass of even a small amount of solid is far larger than that of the individual nuclei that compose it.Thus the degradation of the gamma-ray energy in this case (no phonon creation) is negligible and the gamma ray carries away carries away nearly the entire energy of the decay.The probability of zero-phonon events can be shown (Greenwood and Gibb (1971)) to decrease with increasing gamma-ray energy and with increasing lattice temperature.

The case where the nuclear decay occurs with no phonon creation is known as the Mössbauer effect. The most common application of this effect is the aquisition of Mössbauer spectra,which are obtained as follows. A large number of radioactive nuclei resident in a host lattice decay by release of gamma-rays with a significant proportion of these events being phononless. In this way a highly monochromatic beam of gamma-photons is produced. If this beam impinges upon a solid containing nuclei of the same isotope as the one producing the gamma-rays then these nuclei can resonantly absorb these photons.Slight changes in the nuclear energy levels may occur due to the enviroment of the nucleus, specifically: the s-electron density, the electric field gradient,and the magnetic-dipole moment. Thus if these condtions are different for the source and absorber nuclei then the energy of absorption will differ from the energy of the

gamma-rays. The energy of the photons can be changed slightly by Doppler modulation of the source ,ie by moving the source with respect to the absorber. In this way the energy of absorption can be matched by the impinging gamma-rays and resonant absorption can occur.

A diagram of a typical transmission Mössbauer spectrometer is shown in fig 1.1 . An electro-mechanical transducer subjects the source to a range of velocities to Doppler modulate the source photon energy. The sample absorbs some of the gamma-rays resonantly,the rest impinge upon the detector. In the absence of magnetic fields or electric field gradients , and where the s-electron density of the source and absorber nuclei are identical, a plot of gamma rays counted by the detector versus the Doppler velocity looks like that shown in fig 1.2a . A single absorption line centred on zero Doppler velocity characterizes this spectrum. A difference in s-electron density will result in a shift in this line away from zero velocity (see fig 1.2b). This shift is known as the isomer shift.

The remainder of this discussion will be restricted to the I=3/2 to I=1/2 nuclear transition since this is the transition employed in the ^{57}Fe 14.4 keV Mössbauer effect. This is the most commonly used Mössbauer isotope and the one used in this investigation.

Transition 'b' of fig 1.3 shows how the nuclear levels are shifted to give the isomer shift seen in fig 1.2b . It

is the difference in the I=3/2 and I=1/2 shifts that causes the isomer energy transition shift. This difference is due to the fact that the nucleus has different charge radii in the 3/2 and 1/2 states.

If the absorber nuclei are in the presence of a magnetic field (known as the hyperfine field or H_f) then the degeneracy of the different M_i states is lifted and one obtains the transitions shown in fig 1.3c and the spectrum of fig 1.2c .

If in addition, there is an electric field gradient at the nucleus and the nucleus has a quadrupole moment, the $i=\pm$ 3/2 and $i=\pm$ 1/2 levels are further shifted (see fig 1.3d) and one obtains the asymmetric spectrum shown in fig 1.2d . Fig 1.3e shows a quadrupole interaction in the absence of a magnetic field, demonstrating the lifting of the $M_i=\pm$ 3/2 and $M_i=\pm$ 1/2 degeneracies and fig 1.2e the corresponding spectrum.

The fact that resonant absorption is sensitive to the enviroment of the nucleus makes it useful to the study of magnetism in solids.

The isotope used to produce zero-phonon gamma-rays in ^{57}Fe Mossbauer spectroscopy is ^{57}Co. Its decay scheme is shown in fig 1.4 . The I=3/2 I=1/2 decay has an energy of 14.4 keV.

The splitting of the 1st and 6th lines in the 6 line spectrum of α -iron is about 10.6 mm/s at room tempera-

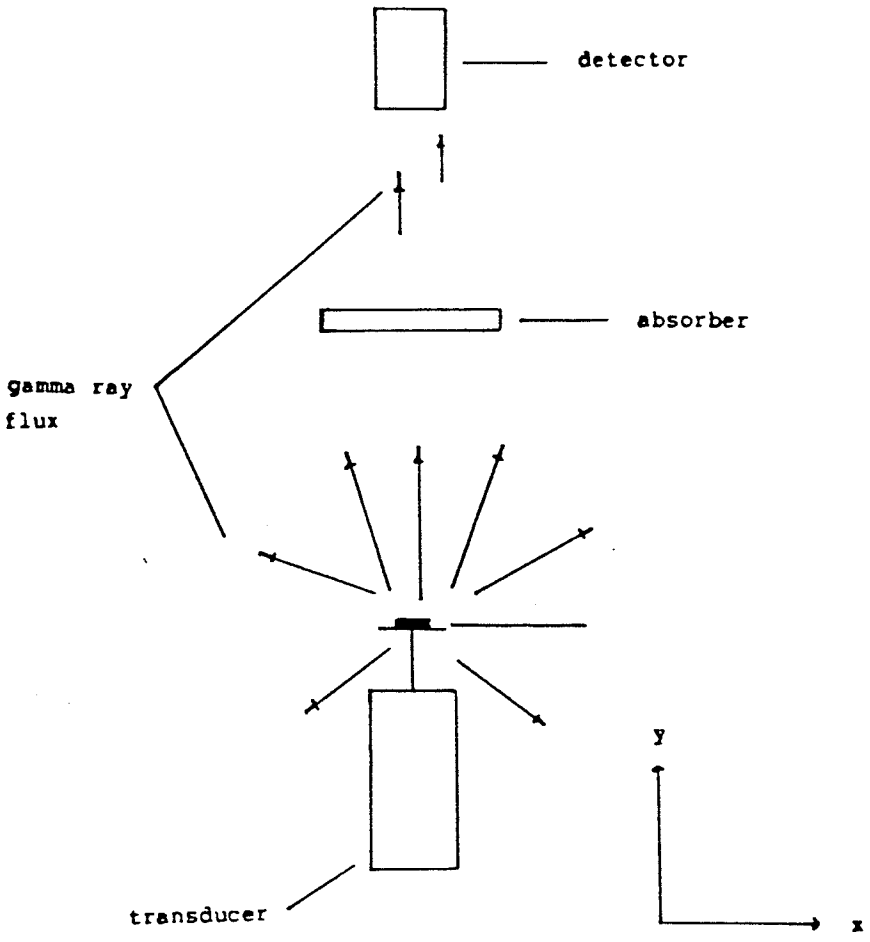

Fig 1.1: Schematic diagram of a basic transmission spectrometer.

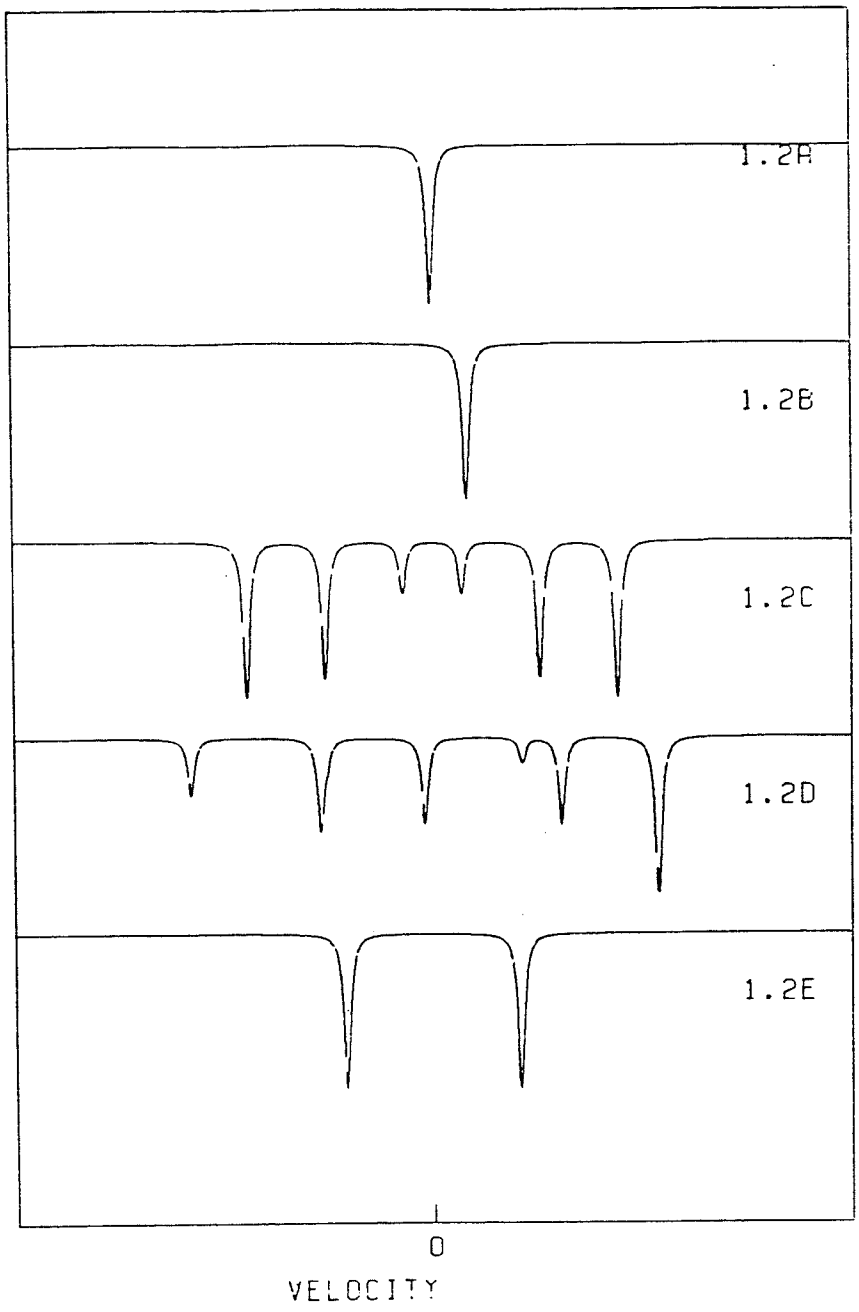

Fig 1.2: The ^{57}Fe spectra resulting from a) no isomer shift, EFG or H_f ,b) with an isomer shift ,c) with an isomer shift and H_f and d) all three of these. Finally, d) shows the spectrum resulting from an EFG only.

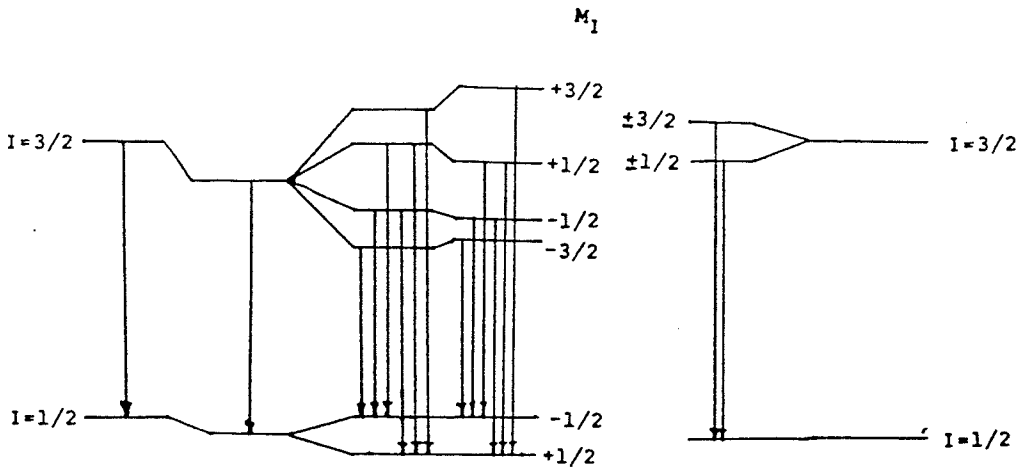

Fig 1.3: The I=3/2 and I=1/2 nuclear levels (with possible transitions) for a) no isomer shift, EFG or H_f ,b) with an isomer shift ,c) with an isomer shift and H_f and d) with all three of these. Finally ,e) shows the levels and possible transitions for an EFG only.

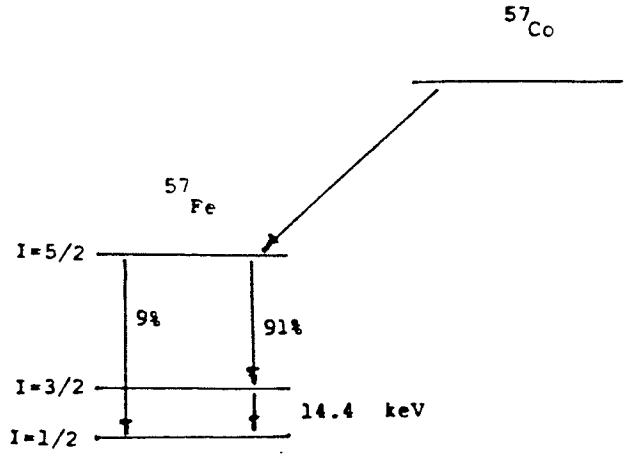

fig 1.4: The decay scheme of ^{57}Co which has a half life of 270 days.

ture. It is to be noted that the fractional difference in energies between these lines (compared to the 14.4 keV zero velocity energy) is $v/c = 3.5 \times 10^{-11}$ where v is the Doppler velocity and c is the speed of light. Thus the Mössbauer spectrum can be used to measure miniscule energy differences (better than one part in 10^{10}).

The I=3/2 exited state has a lifetime of 97.7ns and this gives a Heisenberg linewidth of 0.097 mm/s. Doubling this (since we have both an emission and a subsequent absorption) we obtain a linewidth of 0.194 mm/s which is the linewidth we would ideally obtain in an α -iron spectrum. In practice linewidths of up to 0.28 mm/s are typical for transmission spectrometers in this laboratory due to additional instrumental line broadening.

Not all transitions that constitute the six-line magnetic spectrum have equal probability. These depend upon the angle theta that the gamma-photon makes with the H_f . The resulting relative intensites are (Greenwood and Gibb (1971)):

$$\begin{aligned} &\text{Lines } 1,6 \ldots\ldots\ldots\ldots\ldots 3(1+2\cos^2\theta) \\ &\text{Lines } 2,5 \ldots\ldots\ldots\ldots\ldots 4\sin^2\theta \qquad [1] \\ &\text{Lines } 3,4 \ldots\ldots\ldots\ldots\ldots (1+2\cos^2\theta) \end{aligned}$$

Therefore the magnetic spectrum can be used to obtain information regarding the orientation of the internal magnetization of a magnetic sample.

The concentration of ^{57}Fe in natural iron is 2.17% which is sufficient to obtain Mössbauer spectra in reasonable time provided the concentration of iron in the sample is fairly high.

The above discussion covers those aspects of transmission Mössbauer spectroscopy that are relevent to this investigation. For a more general disscussion the reader is reffered to Greenwood and Gibb (1971).

1.2 CONVERSION-ELECTRON MOSSBAUER SPECTROSCOPY

Excited ^{57}Fe absorber nuclei decay by means of a 14.4 keV gamma-ray in only 9% of cases. In 81% of decays a K-shell conversion electron with kinetic energy of 7.3 keV is released. An L-shell conversion electron (13.6keV) is released with 9% probability and an M-shell conversion electron (14.3 kev) with 1% probability. L-shell events are followed in 70% of cases by a 5.4 keV L-shell Auger electron.It is also possible for K-shell events to be followed by a 6.3 keV x-ray. See Picone and Morrish (1982) for further discussion.

As these resonant electrons travel through the sample they lose kinetic energy due to inelastic scattering from the nuclei of the sample material. Those electrons produced within a few thousand angstroms of the surface are capable

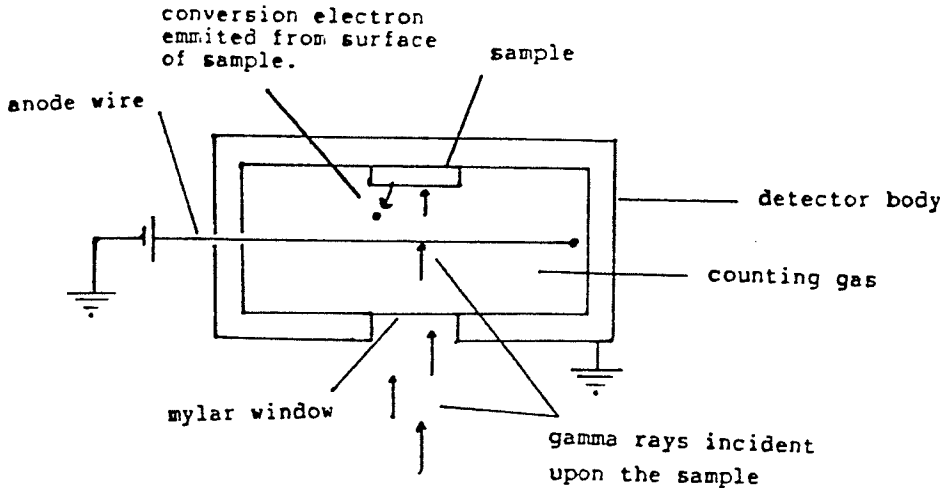

Fig 1.5: Schematic diagram of a proportional counter.

of escaping from the sample, some still possessing significant kinetic energy. Since these electrons are produced by resonant Mössbauer events, the detection of such electrons can be used to form an emission Mössbauer spectrum. This type of Mössbauer spectroscopy is known as Conversion-Electron Mössbauer Spectroscopy, usually abreviated to CEMS. Such spectra are similar to transmission spectra except that they possess emission instead of absorption lines. CEMS spectra are largely representative of the first thousand angstroms of the sample since the resonant electrons created deeper within the sample usually lose all their kinetic energy before reaching the surface. Thus CEM spectra vary from transmission spectra as the latter are characteristic of the entire bulk of the sample.

The easiest way to detect electrons ejected from the surface of the sample is by the use of a proportional counter (see fig 1.5). Gamma-rays enter the counter through the mylar window, some being resonantly absorbed by the sample. Electrons from resonant events that reach the surface with sufficient kinetic energy are capable of ionizing the counting gas that fills the counter. For room temperature CEMS this gas is usually helium. An anode wire is held at high bias with respect to the grounded body of the detector, and this bias causes the charged particles to be accelerated towards the cathode and anode, ionizing further counting molecules in the process. Thus gas amplfication occurs. To pre-

vent a continuous discharge from occuring, a 'quenching' gas such as methane is added to the counting gas in small quantities. After collision with a high energy ion the quenching gas molecules tend to dissociate rather than ionize and in this way the energy of the discharge is dissipated.

The gas ionization event in the counter will produce a current pulse across the output .This can be collected amplified and stored to form a Mössbauer spectrum. Unfortunately the majority of pulses are not due to resonant electrons but to photoelectrons created by the incident gamma-rays in the sample, and these non-resonant events do not contribute to the spectrum but only to a uniform noise across the entire velocity range.

For a full description of the CEM spectrometer used here see ch 2.1

1.3 DEPTH SELECTIVE CEMS

Resonant electrons travelling through the sample have their energies degraded by inelastic scattering from the absorber nuclei. The electrons emerging from a greater depth will, on average, have lost more kinetic energy than those created nearer the surface. The dominant event is the release of the 7.3 K-shell conversion electron. Thus if one

counts electrons only within a narrow energy range one obtains a Mössbauer spectrum that is predominantly representative of a certain range of depths within the sample. Several authors have built electron spectrometers to perform depth selective CEMS (DCEMS) with high energy resolution (see for example O. Massenett (1978)). However, these have inherently poor counting efficiencies because they detect electrons only within small angular limits. The proportional counter on the other hand counts all electrons leaving the surface (provided they have sufficient kinetic energy to ionize the counting molecules) but its resolution is poor. (The proportional counter does in fact possess a linear relationship between electron energy and area of the subsequent current pulse) . Nonetheless some depth selection is possible with the proportional counter (Nakagawa et al (1982)).

With high resolution detectors several spectra of the same sample with differing energy selection can be taken and deconvolution techniques can be employed to generate spectra that are claimed to be truly representative of a particular depth interval within the sample. In doing this the fact that electrons of differing initial energies are being detected must be taken into account. See for example D. Liljequist et al (1979).

With the poor resolution of the proportional counter such deconvolution is not warranted as in this case this is at best a qualitative technique.

One effect,ignored in the disscussion so far, was first described by Tricker et al (1976). The 6.3 keV x-rays mentioned in section 1.2 are capable of producing photoelectrons near the surface of the sample and these electrons contribute to the electron flux near the surface and are detected by the counter. Since the original x-ray was the product of a resonant Mössbauer event,these photoelectrons also contribute to the Mössbauer spectrum.This is in contrast to the photoelectrons created directly by gamma-rays near the surface of the sample which contribute only to the noise.X-rays are not appreciably attenuated by the sample so these contribute a signal that is characteristic of the bulk of the absorber. Therefore it not strictly true that CEM spectra are characteristic entirely of the surface ;there is also a contribution from the bulk due to the x-rays.

Tricker et al (1979) have shown that the deposition of a thin film of an inert (^{57}Fe free) metal such as aluminum on the surface of the sample permits the detection of photoelectrons whilst attenuating the escape of conversion electrons. The greater the depth of the overlayer the larger the contribution to the spectrum from layers deep within the sample. This method can be viewed as an alternative way of obtaining DCEM spectra and was investigated as such in this laboratory. The results of this are reported in ch 3.3.

1.4 THE FORMATION AND STABILITY OF AMORPHOUS THIN FILMS.

An amorphous solid can be defined as one in which there is no periodic crystal structure. This implies a distribution of nearest-neighbour distances and hence also of bond lengths. This is obviously a metastable state since the condition of minimum energy for a solid occurs when it is in its crystalline form. However, the stability of many amorphous materials is great enough so that they remain in their non-crystalline form for a long time (at least several hundred years).

Thin amorphous films can be formed by thermal evaporation in a vacuum or by sputtering. The accretion of material upon the substrate is usually only a few angstroms per second, and consequently the thermal energy of the evaporant atoms is quickly dissipated with no appreciable increase in surface temperature. Thus, no significant relaxation of newly arrived evaporant atoms occurs and an amorphous solid results. Rare earth-transition metal amorphous thin films can be produced in the amorphous state with the substrate held at room temperature. For a detailed discussion of the stability of non-crystalline solids the reader is referred to Wang and Merz (1977).

1.5 RARE EARTH TRANSITION METAL AMORPHOUS THIN FILMS.

Sputtered and evaporated RE-TM thin films (where RE=Gd,Ho,La, Dy,Y,Tb and Tm=Fe,Co,Ni) are ferrimagnetic. The TM-TM magnetic interaction is due to direct exchange betwen d-electrons. In contrast, the RE-RE and RE-TM interactions are of the RKKY type; ie they arise due to the polarization of conduction electrons. The RKKY interaction occurs by exchange between the d-electrons and the conduction electrons of an atom. Since the latter are free to move from ion to ion, they can polarise the d-shell of neighbouring atoms. In this manner indirect spin correlation is produced and maintained.

Evaporated amorphous thin films of GdFe have been observed by electron microscopy (Dirks and Leamy(1978)) to have a microstructure consisting of high density columnar structure of diameters in the range of 50-250 Å interspaced with lower density regions of thickness 10-25 Å. The existence of columnar microstructures in evaporated amorphous materials is explained by these authors in terms of self shadowing of the evaporant flux. Henderson et al (1974) have demonstrated this for single species evaporation by computer simulation. A low mobility of condensed evaporant flux is a requirement for both the amorphous state to result and for the self shadowing to occur. Dirks and Leamy have extended this to

the case of two evaporant species and have shown that the columns are rich in one species and the surrounding areas rich in the other.

Evaporated and sputtered RE-TM films have been observed to possess a magnetic moment perpendicular to the plane of the film. This perpendicular anisotropy has been the subject of much discussion (Tsunashima et al (1980)). Anisotropic atom-pair ordering, stress-induced anisotropy due to the constraint of the substrate, shape anisotropy due to anisotropic microstructure , and the anisotropic interaction of non-S-state rare earth ions have been proposed as possible causes for the observed magnetic behaviour. In the case of evaporated Fe-Gd the dominant mechanism appears to be shape anisotropy (Dirks and Leamy). The long axis of the columnar growths observed by Dirks and Leamy is in the perpendicular direction and thus demagnetization energy is minimized for the moment lying along the film normal.

The lines of a simple crystalline substance such as α-iron are Lorentzian in shape .In amorphous substances the hyperfine field felt by the nucleus varies from atom to atom because interatomic distances have a range of values as opposed to fixed ones in the case of crystals. Thus one would expect Mössbauer spectra of amorphous solids to be composed of a large number of Lorentzian lines summed according to some distribution function. Previous results on amorphous Gd-Fe films are consistent with this view (Chappert (1979))

with all spectra displaying the broad lines characteristic of a range of H_fs. Chappert also mentions that a small contribution to line broadening occurs due to a small, randomly orientated EFG.

CHAPTER TWO: EXPERIMENTAL

2.1 APPARATUS.

The CEM spectrometer used in this investigation is shown diagramatically in fig 2.1 . The source consisted of ^{57}Co radioactive nuclei in a rhodium host and produced highly monochromatic radiation. Doppler modulation of this radiation is provided by the motion of the transducer. The radiation enters the proportional counter through its mylar window and impinges upon the sample. A 60 micron diameter tungsten wire held at 1000 V bias with respect to ground potential served as the anode of the counter. Helium was used as a counting gas with 4% methane added to act as a quenching agent. This mixture was flushed continuously through the chamber at 0.16 cc/s.

The preamplifier converts the current pulses produced by the detector and converts them into voltage pulses and amplifies them. Further amplification (typically a factor of 200) occurs at the main amplifier. Then the single channel analyzer selects those pulses that lie within certain preselected voltage limits and outputs a 5 volt TTL pulse for each pulse within these limits.

This voltage discrimination is useful in eliminating low-energy pulses which are mainly due to non-resonant events in the detector and have negligible signal content. It is also useful in obtaining DCEM spectra, as explained in chapter 3.4.

The proportional counter has an intrinsic capacitance that results in a sinusoidal modulation of about 200 hz on the preamplifier output. This reduces the effectiveness of the SCA voltage discrimination. A high-pass filter was installed after the preamplifier to attenuate the ripple whilst allowing the signal pulses to pass unimpeded.

Output pulses from the SCA are accumulated by the MCA and stored to form the Mössbauer spectrum.

Two transducer velocity waveforms are currently in common use in Mössbauer spectroscopy ;the sawtooth and triangular forms. These are so named because this is the shape of the velocity function with respect to time (see fig 2.2). The transducer function generator produces the voltages required to induce the desired movement of the transducer.When the MCA starts a new sweep it sends a pulse to the function generator to initiate a new transducer cycle thus insuring that the MCA and transducer are in synchronization. Each of the MCA's 512 channels are open for an equal amount of time each sweep. If the transducer velocity is linear with respect with time (as it obviously is in the triangular and sawtooth cases) then there is a linear relationship between MCA channel number and transducer velocity.

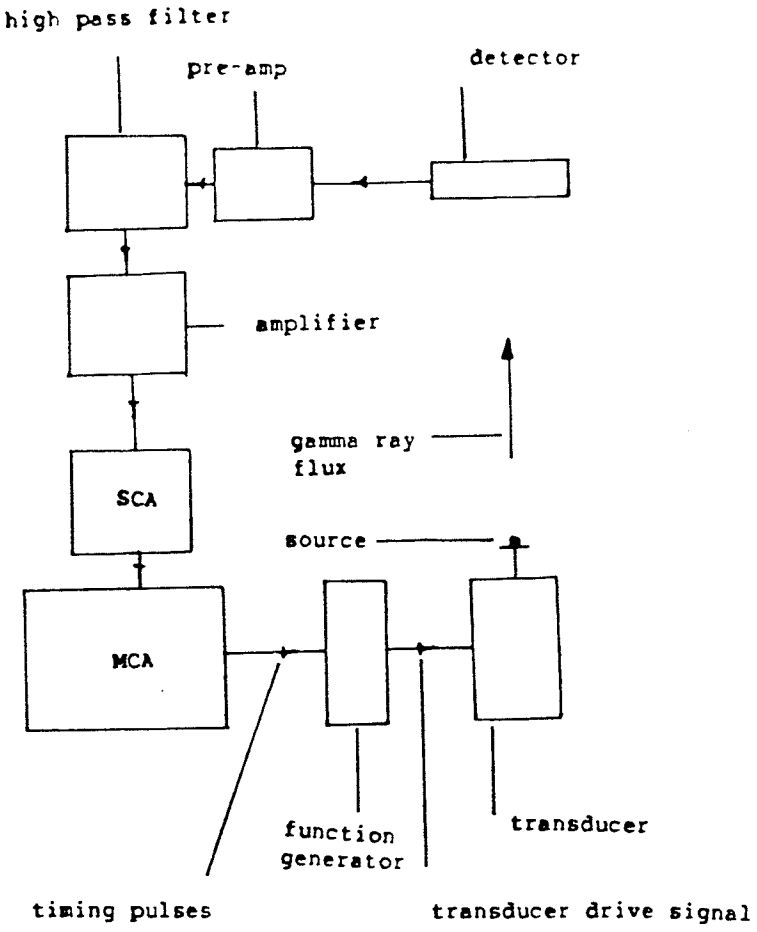

Fig 2.1 Schematic diagram of the CEM spectrometer used in this investigation.

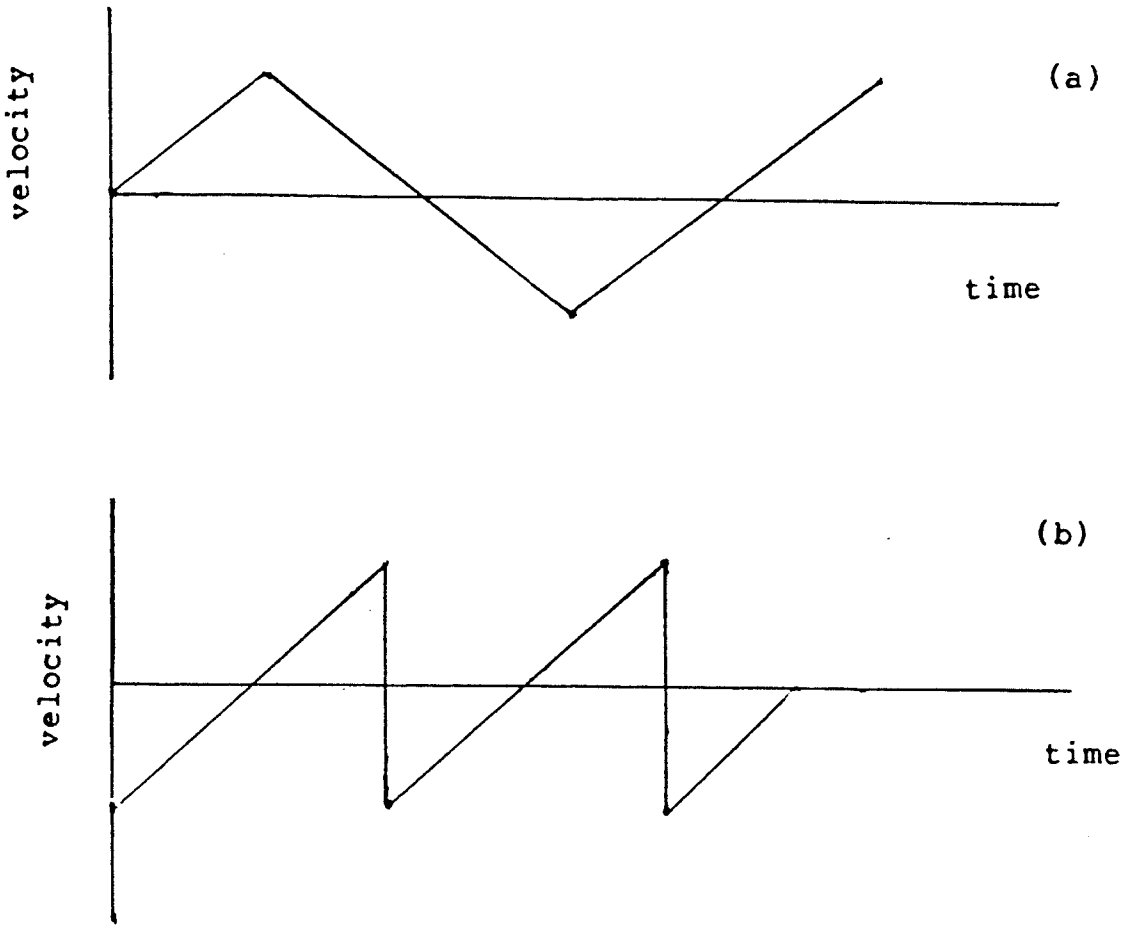

Fig 2.2: Velocity waveforms of a) the triangular and b) the sawtooth modes.

As can be seen from fig 2.2, the spectrometer collects two spectra per cycle in the triangular mode as opposed to one for the sawtooth case. Pairs of channels that share a common velocity can have their contents added thus forming a composite spectrum.This procedure is known as "folding" due its obvious geometrical interpretation.

The source to sample distance is not constant but is a function of transducer velocity. This produces a parabolic background due to the inverse square law of radiation intensity. The folding of a triangular spectrum cancels this background. For this reason the triangular mode has an advantage over the sawtooth since in the latter case the curvature must be numerically estimated and substracted from the spectrum. A small error in this estimation will result in large errors in line intensities . This is particularly severe if line intensities are small as in our case where they are typically smaller than 1%. For this reason it was elected to use the triangular mode in every spectrum presented here.

The window settings were set to aproximately maximize the time independent signal to noise ratio. This quantity can be derived as follows:

$$signal=C_m - C_b$$

where Cm is the total counts at the crest of a peak and Cb is the baseline count. Also:

$$noise=\sqrt{C_b}$$

This expression arises because the arrival of signal pulses in a Mössbauer spectrum occur at random time intervals. The standard distribution of the scatter in the baseline equals C_b as deduced by Poisson statistics which such random systems obey. Therefore;

$$S/N = (C_m - C_b)/\sqrt{C_b}$$

$$= I\sqrt{C_b}$$

where I is the fractional intensity.

I is time independent, but C_b is proportional to t, the time taken to acquire the spectrum. For this reason the time independent S/N can be written:

$$S/N = I\sqrt{C_b}/\sqrt{t}$$

With this optimization, spectrum acquisition will be the most efficient. Although this optimization was done for α-iron it was not expected to change significantly for the experimental samples used here. Optimization was only aproximate since the process of optimization takes considerable spectrometer time and S/N was expected to be within a few percent of its maximum anyway.

2.2 LEAST SQUARES FITTING

After the collection of a Mössbauer spectrum the contents of the MCA memory were transferred to a disk file on the University of Manitoba Amdahl computer where a least squares fitting program written by Dr. R.J. Pollard was used to fit a theoretical curve to the experimental spectrum. Such fitting could be done subject to constraints on the theoretical spectrum such as fixed line positions, widths and intensities.

Calibration spectra were taken before and after every experimental spectrum in order to monitor any changes in the transducer's dynamic characteristics. Velocity versus MCA channel number calibration was done by taking a spectrum of α-iron whose six line positions are known to great accuracy. The iron spectrum was fitted by the least squares program ,each line constrained to have its known position.

The velocity (v) versus MCA channel number (n) function was assumed to be linear:

$$v = a + b.n \qquad [1]$$

with the constants a and b determined by the fitting program. Any nonlinearity in the transducer's velocity function will result in a poor correspondence between the theoretical and the experimental spectra. The values of a and b

were assumed to be valid for experimental spectra taken immediately before and after the calibration.

As well as this the iron calibration spectrum was used to find the centre of the iron spectrum so as to provide a convenient reference for isomer shifts (the actual zero velocity position was not found since it is usual to report isomer shifts with respect to the centre of the α-iron spectrum). Also, the folding centre was left as a fitted parameter(ie allowed to vary) so an accurate value could be obtained and used on subsequent experimental spectra.

2.3 ANGLE EFFECTS

Spectra of good resolution took excessive time to collect due to the weak source that was employed for the majority of spectra. In order to obtain CEMS spectra in reasonable time the source to sample distance was reduced to 5 cm. This is several times smaller than than for typical transmission geometries . At this close distance an iron spectrum of good resolution could be obtained in about 24 h.

Small source to sample distances mean that gamma-rays impinging upon the edges of the sample strike at angles that are significantly different to the sample normal. This can have two effects. Firstly the contribution to the spectrum

from the edges will have different relative line intensities due to the different gamma-ray H_f angles.Calculations,presented in appendix A, show this to be negligible in our case . Secondly, and more importantly, the non-normal gamma rays have only the normal conponent of their velocity Doppler modulated and this results in line broadening and changes in position.

Barra and Barag(1980) have discussed this second effect and have shown that the line width is equal to:

$$\Gamma = v^2(1 - \cos \alpha) + \Gamma_0^2$$

where v is the line position in units of Doppler velocity, a is the angle defined in fig 2.3 and Γ_0 is the $\alpha = 0$ line - width. The shift of line positions away from their $\alpha = 0$ position v towards the centre of the spectrum is give by these authors as

$$\Delta v = v(1 - \cos \alpha)/2 \qquad [2]$$

The line widths computed for α -iron for the CEM spectrometer used here (assuming $\Gamma_0 = 0.28$ mm/s) is 0.35mm/s for lines 1 and 6,0.30mm/s for lines 2 and 5, and 0.28 mm/s for lines 3 and 4.

The line broadening does not degrade the value of the calibration spectra since the line positions can still be accurately matched by the fitting program. The experimental samples used here were not as wide as the iron sample used in

calibration and with the corresponding decrease in the value of α the 1 and 6 lines were only broadened by about 4% and the (3,4) lines by a negligible amount(the (2,5) lines have zero intensity).

The change in line positions will have an effect on H_f measurements and on calibrations. According to equation 2, the calibration constant obtained from the iron spectra will be 2.1% too small for our geometry. The experimental spectra will display line splittings of about 1% smaller than the α =0 case. Therefore the observed H_f s of the experimental spectra will be:

$$2.1 - 1 = 1.1\ \%$$

too small in each case. The small magnitude of this error (about the same size as the uncertainty in each measurement) makes it of little consequence and the data presented in this report have not been corrected for this effect.

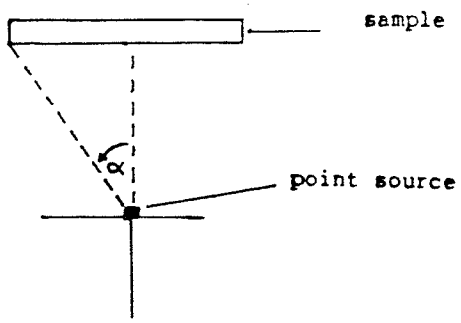

Fig 2.3: Definition of the angle α . See the discussion in chapter 2.3 .

CHAPTER 3: RESULTS.

3.1 CALIBRATION SPECTRA

An α-iron spectrum, typical of those taken during this investigation is shown in fig 3.1 . The points are the experimental data points and the full line is the theoretical curve. The (2,5) lines have greater intensity than the (1,6) lines, indicating a predominance of in-plane magnetisation.

All spectra presented here were taken with a triangular velocity drive and subsequently folded. The folding centre was left as a variable parameter in the calibration spectra and the resulting value used on the subsequent experimental spectrum this time constrained to this value. No evidence of nonlinear baselines were observed after folding.

3.2 INTEGRATED CEM SPECTRA OF AMORPHOUS FE:GD THIN FILMS.

Integrated CEM spectra of 5000 Å thick amorphous

Fe_xGd_{100-x} films (x=78,77,72,66) were obtained at room temperature. These spectra are displayed in fig 3.2 . Also shown is the electron energy profile of the proportional counter with the aproximate SCA gate settings used in these spectra. These settings aproximately optimized spectrum aquisition, as explained in ch 2.1 .

These spectra all display the six-line magnetic spectrum with the (2,5) lines having negligible intensity, indicating that the samples are magnetized perpendicular to the film plane. This perpendicular anisotropy, and the very broad lines, are consistent with previous results on these films (Heiman and Lee (1975)).

Each spectrum is fitted to a range of H_f s that follow a Gaussian distribution. The lineshapes of the spectra resulting from each H_f were Lorentzian.

It is to be noted that this method differs from the that of employing singlets and doublets (of Gaussian or Lorentzian lineshape) whose parameters are not constrained by theoretical considerations. The many constraints implied by a theoretical model means that good fits are not always possible. This is in contrast to an empirical approach that can always be made to give good fits if one is prepared to ignore theoretical considerations.

The advantage of fitting as it was done here is that correspondence to or deviation from theory is immediately visu-

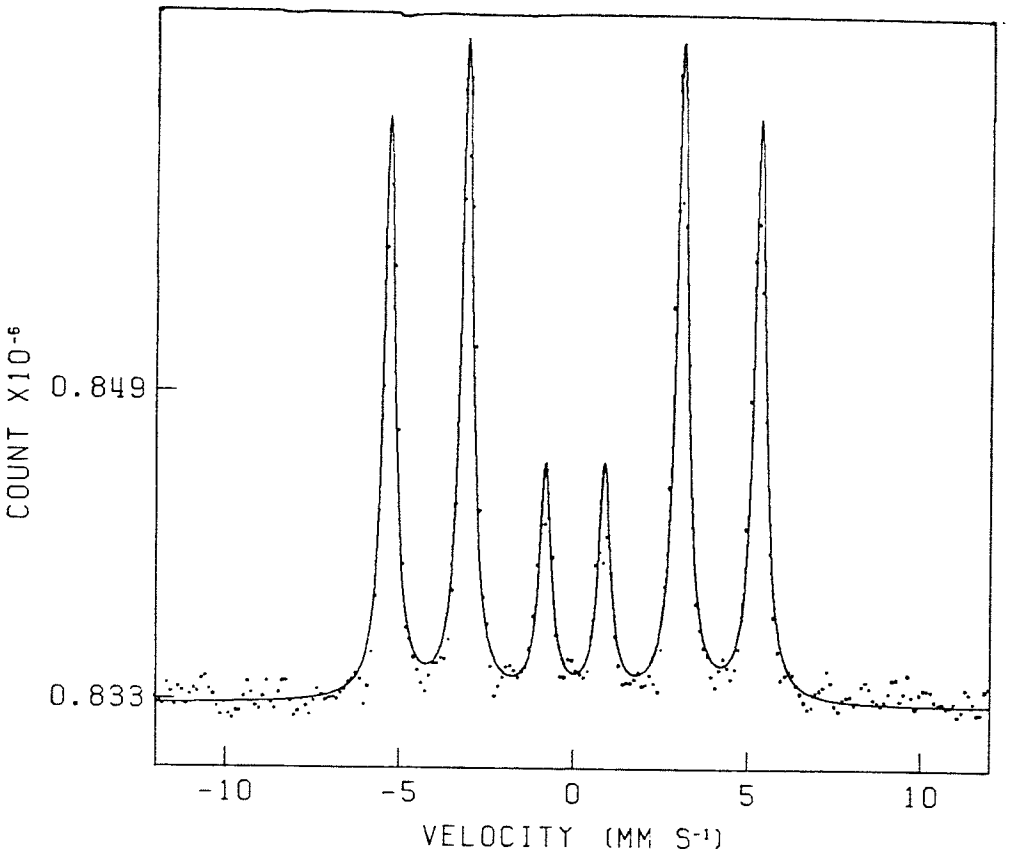

Fig 3.1: Typical α-Fe calibration spectrum taken during this investigation.

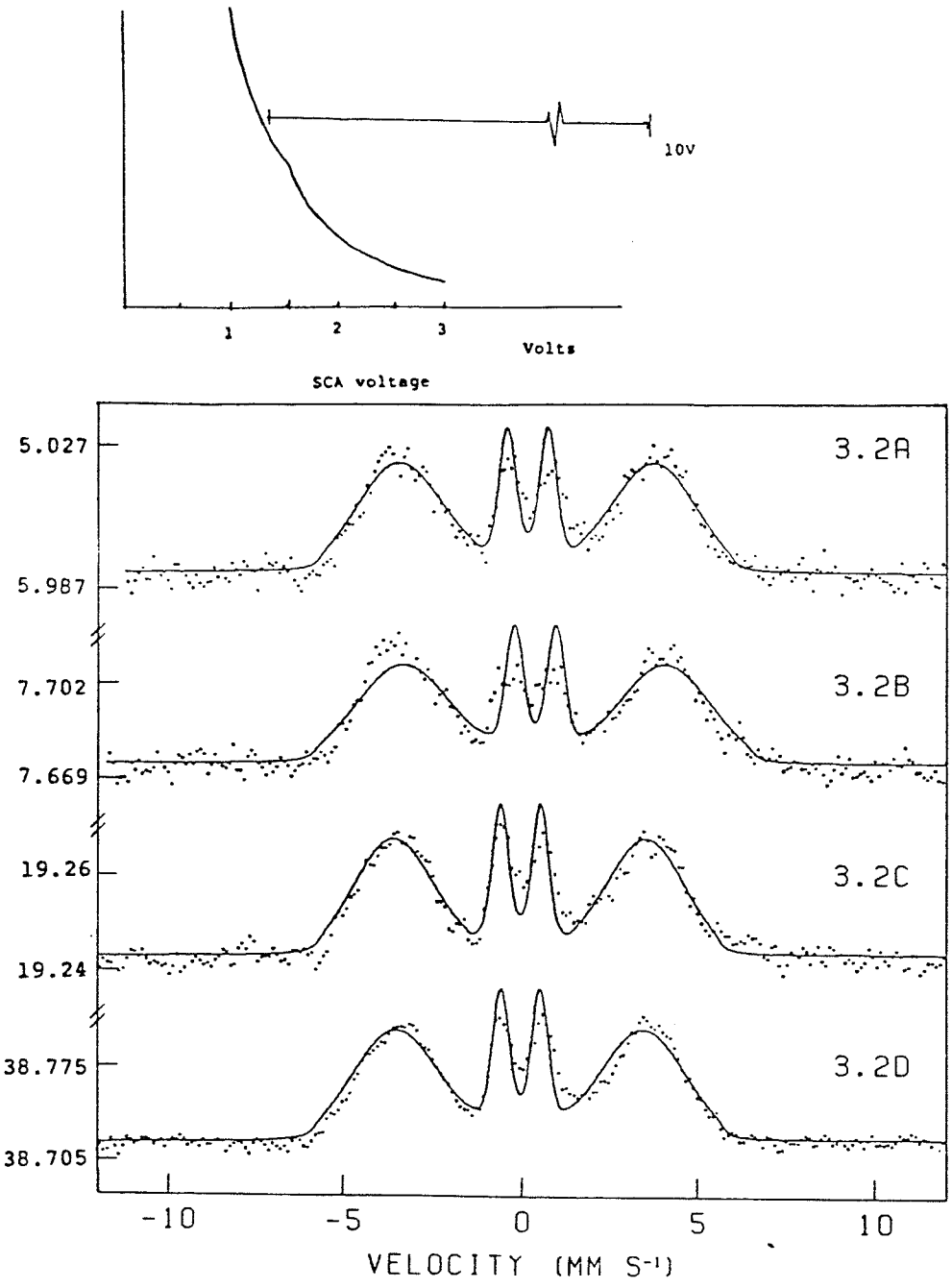

FIG 3.2 Integrated spectra of FexGd100 X where X a)=78,b)=77,c)=72,d)=66. Also shown is the window setting used.

ally obvious from a plot of the theoretical curve superimposed on the experimental data. The empirical method requires calculation of the theoretically expected values of the various parameters which are then compared to the experimental parameters as measured by the numerical fit.

It is to be borne in mind that in the empirical approach, the H_f -gamma ray angle (theta) cannot be calculated by simply substituting the relative line intensities into eq 1.1 . However, with the method presented here,theta is a fitted or constrained parameter from which the correct line intensities are calculated and thus is always available.

It is obvious that the line shapes of the fits given here will be neither Gaussian nor Lorentzian but are a function of σ^1 and the width of the individual Lorentzians.

The theoretical curves of fig 3.2 fit the experimental data fairly well, so it can be concluded that a Gaussian distribution of H_f s being present at the sample nuclei is consistent with these results.

Chappert (1979) states that a small randomly orientated EFG is present in RE-TM films. This results in a slight and equal broadening of all lines of a Mossbauer spectrum. This is opposed to the broadening due to a range of H_f s which broadens lines in proportion to their distance from the spectrum center. Since the EFG was assumed to be zero in the fits presented here, poor correspondence between the data and the theoretical curves would result if indeed there was

1 σ = the standard distribution of the Gaussian.

a EFG present. Inspection of fig 3.2 shows that in each spectrum the (3,4) lines are broader and less intense than the theoretical curve indicates they should be. This is exactly the type of broadening that is consistent with a small, randomly orientated EFG. Therefore the results presented here are evidence for Chappert's claim.

Isomer shifts of no more than $\sim$0.3 mm/s are observed here which is roughly the magnitude of the error to be expected in this quantity with this spectrometer. Negligible isomer shift has been found to be characteristic of RE:TM films in previous studies (Chappert (1979),Heiman and Lee (1975)) so this result is to be expected.

The $\overline{H}_f^{1}$ versus iron concentration is shown in fig 3.3 . $\overline{H}_f$ increases monotonically with x as is to be expected. This graph is similar to Heiman and Lee's results for 4.2 K except that the $\overline{H}_f$ is slightly smaller in each case as is reasonable for room temperature spectra. The similarity between the transmission and CEMS results is not surprising since CEMS probes essentially a depth of a few thousand angstroms and these films are only 5000 Å thick. So,in both cases, the spectra are mainly representative of the 'bulk' of the film , in so much as any film with interfaces 5000 Å apart can be considered bulk material.

The electron profile shown in fig 3.2 is similar to that obtained by Nakagawa et al (1982) for a proportional counter used for CEMS. In particular, the small peak at 1.5 volts

1 $\overline{H}_f$ = average H_f

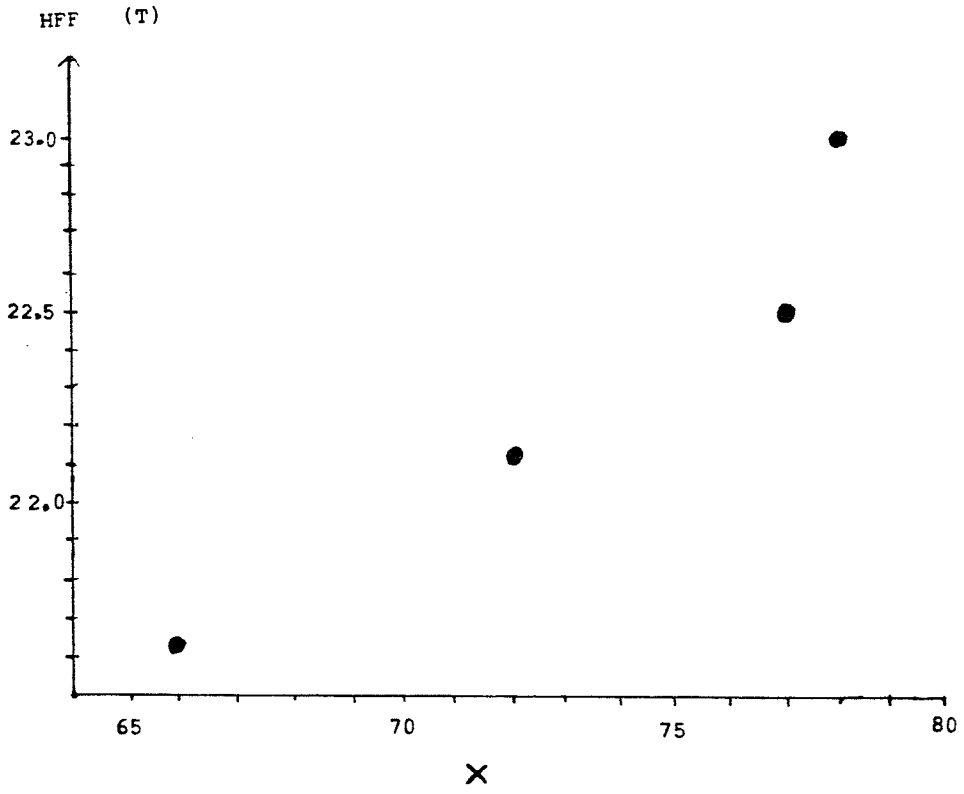

Fig 3.3: Hff versus x for FexGd100-x with x=78,77,72,66.

	Fe /S.S.
S.S. + Fe	0.155
S.S. + Fe + Al	0.086

showing that the relative signal strength does indeed vary as expected.

3.4 DCEM SPECTRA BY DISCRIMINATOR LEVEL SETTING

A sample consisting of a stainless steel substrate with a 200 Å surface layer of iron was produced in the same manner as described in the previous section. Two spectra of this sample were taken with different window settings. The window settings are shown in fig 3.5 . The spectra were similar to those produced by overcoating and were roughly the same statistical quality. The ratio of line intensities of the two layers was:

Window	Fe(1,6) / S.S.
A	0.23
B	0.54

showing that the the surface to bulk signal does vary with window setting in the expected manner.

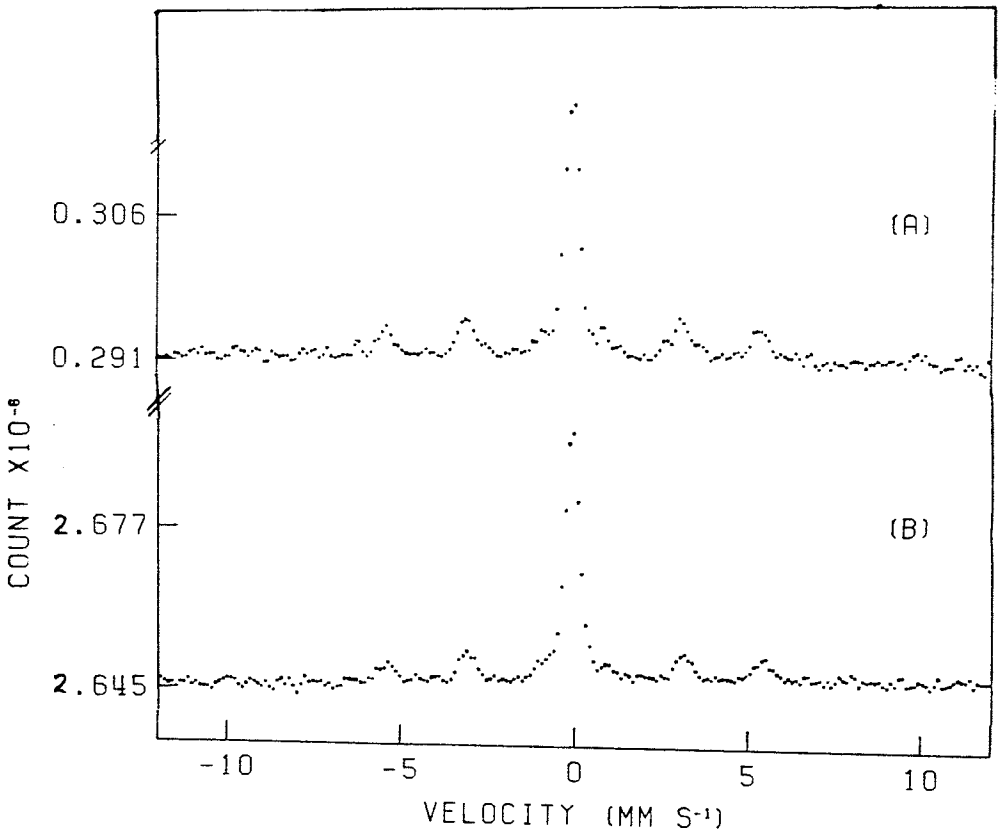

Fig 3.4: Integrated spectra of a) stainless steel + iron and b) stainless steel,iron and 2000 angstroms aluminium.

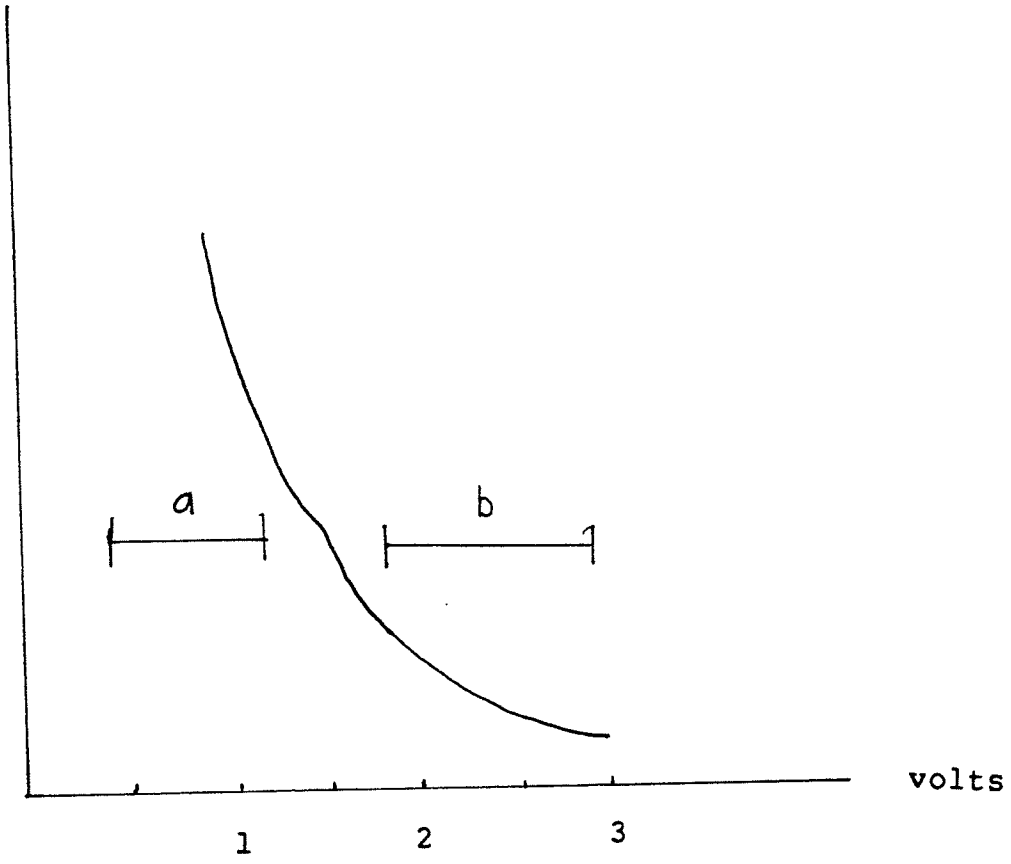

Fig 3.5: Window settings used to obtain the two DCEM spectra of iron-stainless steel.

The results obtained on the Fe-SS sample indicate that both the window setting and the inert overlayer method can distinguish between surface and bulk signals. The thickness of the aluminum used here (~200 Å) is considerably less than that used by either Nakagawa et al (1982) (~600 Å) or Tricker et al (1000 Å). Consequently the change in Fe:SS signal ratio possible by varying the window setting was not as large as Nakagawa et al achieved. As well, a smaller change in this ratio was observed than reported by Tricker et al for similar depths of aluminum. However, it may be concluded that surface layers of less than 200 Å can be identified by both of these methods.

DCEM spectra by selective window setting of $Fe_{77}Gd_{23}$ and $Fe_{72}Gd_{28}$ are presented in fig 3.6. Also presented is the spectrum of $Fe_{77}Gd_{23}$ after 2000 Å of aluminum was deposited on its surface. The absence of any marked differences between the various DCEM spectra presented here indicate that these spectra are largely homogeneous with depth. There is no difference in the $\overline{H}_f$ found here and that found in the integrated spectra. There is some difference found in σ but this is small and not correlated with depth.

There appears to be no evidence of more than one distribution of sites in any of the integrated spectra. Howerver, both the high and low window spectra of Fe Gd seem to arise from two

distributions of sites about two distinct average H_f s with the one with the larger $\overline{H}_f$ being dominant. This is however liable to be only an artifact since it is hard to see how two distinct $\overline{H}_f$ s could be present in both the high and low window spectra and be absent in the integrated spectra.

As with the integrated spectra the (3,4) lines are not as well fit as the (1,6) lines , again indicating the possibility of a random EFG. The fact that the (3,4) fits are neither better nor worse than those previously presented indicates that there is no appreciable change in this EFG with depth.

3.5 ANNEALING EXPERIMENTS

Two amorphous thin film samples: $Fe_{78}Gd_{22}$ and $Fe_{71}Gd_{29}$ were each annealed at sucessively higher temperatures, with a Mössbauer spectrum taken after each heating. Initially, both samples were annealed by Dr. R. Soohoo at UC Davis at 250° C for 24 hours. Subsequent to this the samples were further annealed in this department at higher temperatures for one hour using the furnace and vacuum facilities of Dr. P. Gaunt.The annealing done by Dr. Soohoo was done at a pressure of 10^{-8} Torr whereas the annealing done here was at

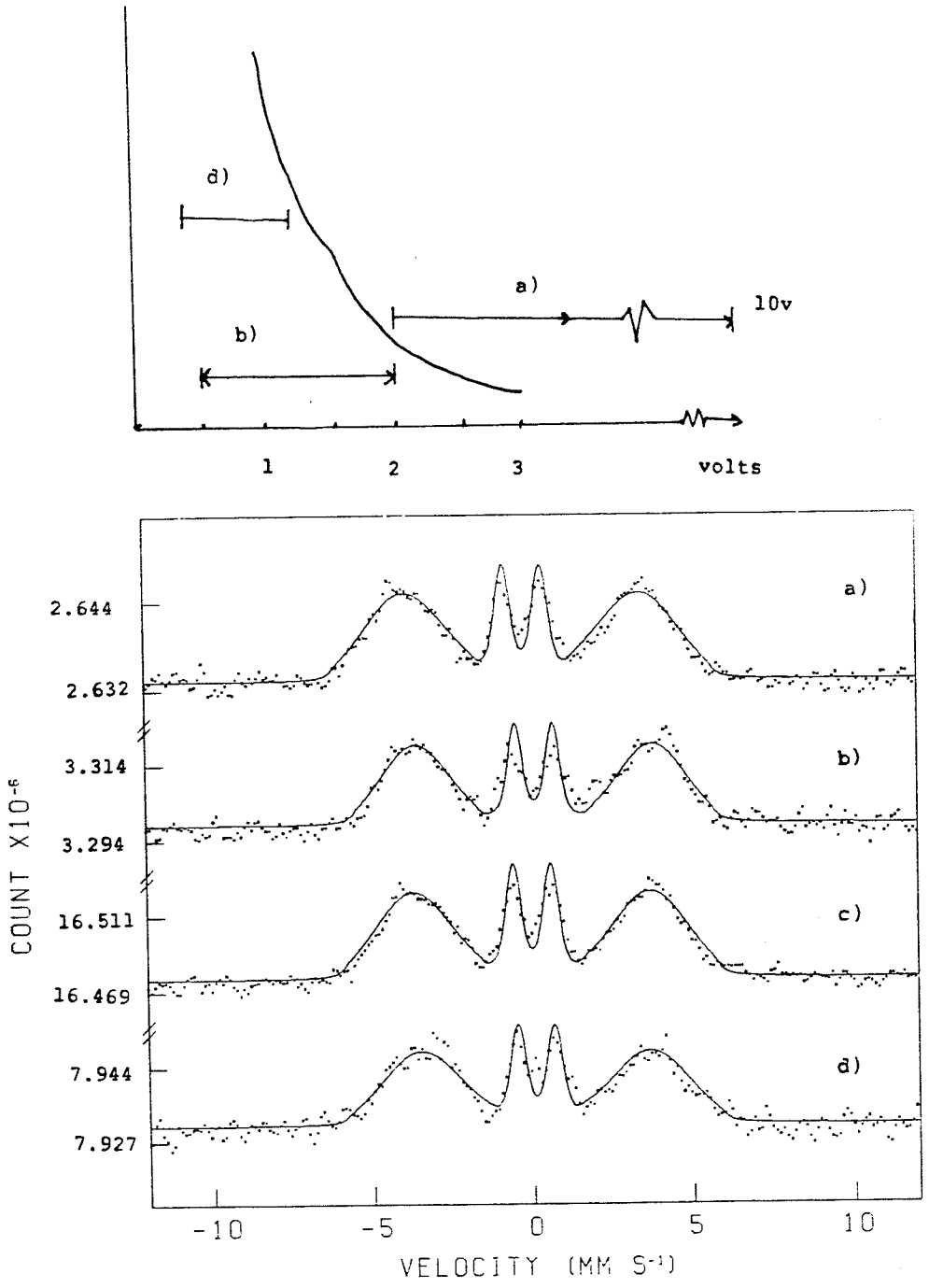

Fig 3.6: Dcem spectra of $Fe_{77}Gd_{23}$ with a) a high window setting, b) a low window setting and, c) with 2000 a Al deposited upon the surface. Also shown is a low window spectrum of $Fe_{72}Gd_{28}$. Refer to the energy profile for the window settings used in each case.

10^{-6} torr. However the sample chamber was repeatedly flushed with helium gas and re-evacuated prior to annealing at the higher pressure. This was done to minimize the risk of oxidising the sample.

The resulting spectra are shown in fig 3.8 .Details of the theoretical curves used to fit this data is shown in table 1.

Annealing at 250°C appears to have made little difference to the spectra apart from a slight decrease in $\overline{H}_f$ and a slight increase in σ . It is apparent that some atomic rearrangement is taking place but no significant crystallization has yet occured.

The annealing of $Fe_{78}Gd_{22}$ at 350° C resulted in in an amorphous phase with a sharply reduced $\overline{H}_f$, and a single site phase with the same H_f of alpha-iron. The obvious interpretation is that alpha-iron is precipitating out with the reduction of the $\overline{H}_f$ of the amorphous phase indicating that Gd is not doing the same to any great extent.

$Fe_{71}Gd_{29}$ displays almost the same spectrum as after annealing at 300° C as did $Fe_{78}Gd_{22}$ after heating to 350° C . The main difference is that the H_f of the single site phase is about 5% smaller than alpha-iron Therefore, in this sample, some Gd has precipitated out to form an crystalline alloy with Fe. The final annealing of this sample at 350°C shows that the crystalline phase now consists of an Fe-Gd alloy . The distribution of H_f s in this phase indicates

that this is indeed an alloy and not a compound, the latter being characterised by a finite number of discrete H_f values. The $\overline{H_f}$ of the amorphous phase has increased once more to roughly its preannealing value. It is therefore likely that the ratio of Fe to Gd in this phase is about 71:29 and therefore the same in the crystalline phase.

In order to get a good fit it was found necessary to fit the crystalline phases assuming theta substantially greater than zero (see table). The perpendicular anisotropy characteristic of the amorphous phase was therefore not present in the crystalline alloy.

It was found that the as deposited samples had electrical conductivities that were too low to be measured by an conventional multimeter. However, after annealing the films displayed a significant conductivity (about 2000 ohms using ordinary needle probes 1.0 cm apart). The low initial conductance is consistent with the microstructure described by Dirks and Leamy. The low density material surrounding the columns would account for such electrical behaviour. It seems apparent that from these measurements that the microstructure is destroyed by annealing.

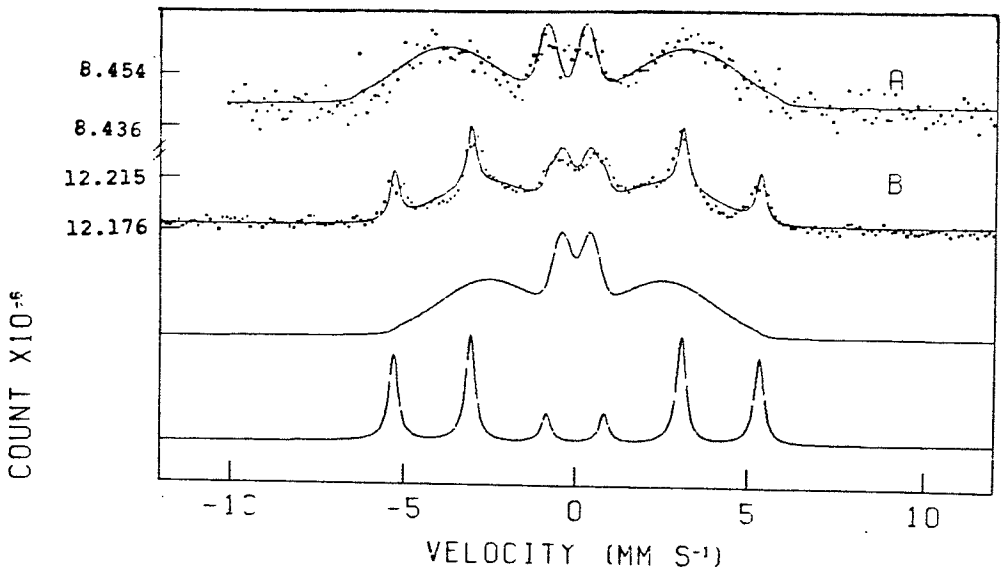

Fig 3.7: CEM spectra of Fe78Gd22 annealed at a) 250° C b) 350° .The two conponents of b) are also shown separately.

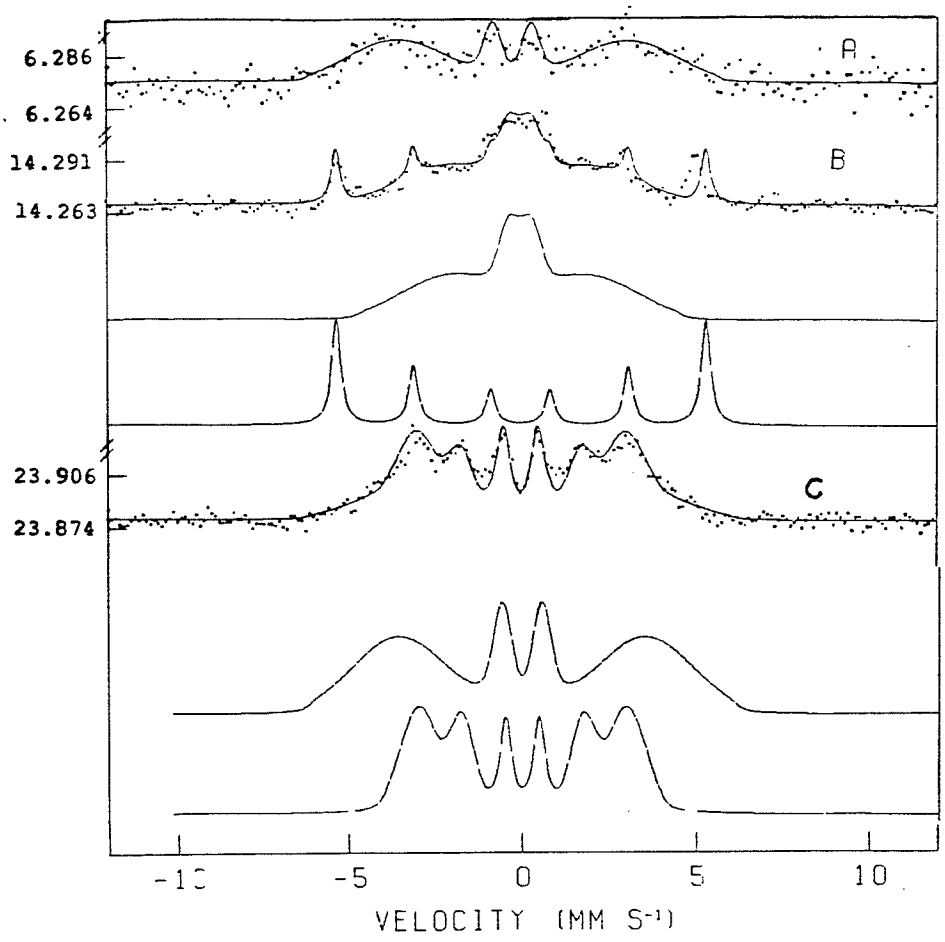

Fig 3.8: CEM spectra of Fe71Gd29 annealed at a) 250° C b) 300° c) 350° .The conponents of b) and c) are also shown.

TABLE 1

Details of annealed films

	PHASE 1	PHASE2
$Fe_{71}Gd_{29}$		
250°C for 24 h. $p=10^{-8}$ torr	H_f =21.4[1], σ=7.8 θ=19°	
300°C for 1 h. $p=10^{-8}$ torr	H_f =12.0, σ=8.5 θ=0°	H_f =33.0, σ=0.0 θ=50°
350°C for 1 h. $p = 10^{-6}$ torr	H_f =22.0, σ=8.0 θ=0°	H_f =18.5, σ=3.0 θ=52°
$Fe_{78}Gd_{22}$		
250°C for 24 h. $p= 10^{-8}$ torr	H_f =22.1, σ=8.1 θ=14°	
350°C for 1 h. $p = 10^{-6}$ torr	H_f =16.0, σ=8.5 θ=0°	H_f =33.0, σ=0.0 θ=80°

1 HFF and σ in units of Tesla.

CHAPTER 4: CONCLUSION.

The results presented here successfully supplement the transmission Mossbauer spectroscopy previously performed on Fe-Gd films. Depth selection was successfully attempted and the results indicate that there is no appreciable change in magnetic properties with respect to depth. The conductivity measurements support the existence of microstructures in the as deposited films, which is destroyed upon annealing.

Annealing showed the precipitation of metalic iron followed by the formation of a crystalline Fe-Gd solution in the case of $Fe_{71}Gd_{29}$. The formation of a solid solution in the other sample ($Fe_{78}Gd_{22}$) was not observed at the temperatures used here. The two films were on opposite sides of a stoichiometric composition ($Fe_{75}Gd_{25}$) and this is probably the main reason for their difference in behaviour.

APPENDIX: ANGLE EFFECTS

In this appendix we examine the effect of non-zero α on relative line intensities. This is in addition to the change in Doppler modulation discussed in section 2.3 .

For simplicity we consider the case where the magnetisation of the sample is perpendicular to the plane of the film, a condition we find is satisfied for most of the samples analysed in this project. Consider a point source with and d defined as in fig a.1 . Now the line intensities will be:

$$I_{1,6} = \frac{\int_0^{\alpha} d(1+\cos^2\theta)\, d\theta}{\int_0^{\alpha} d.d\theta}$$

and

$$I_{2,5} = \frac{\int_0^{\alpha} d\sin^2\theta\, d\theta}{\int_0^{\alpha} d.d\theta}$$

When integrated this yields:

$$\frac{I_{2,5}}{I_{1,6}} = \frac{4 \ln \tan[\pi/4 + \alpha] - \sin\alpha}{3 \ln \tan[\pi/4 + \alpha] + \sin\alpha}$$

This function is plotted in fig a.1 . α is in the range of 12-16^{o} throughout this investigation and thus this effect

is negligible and has not been taken into account for spectra presented here.

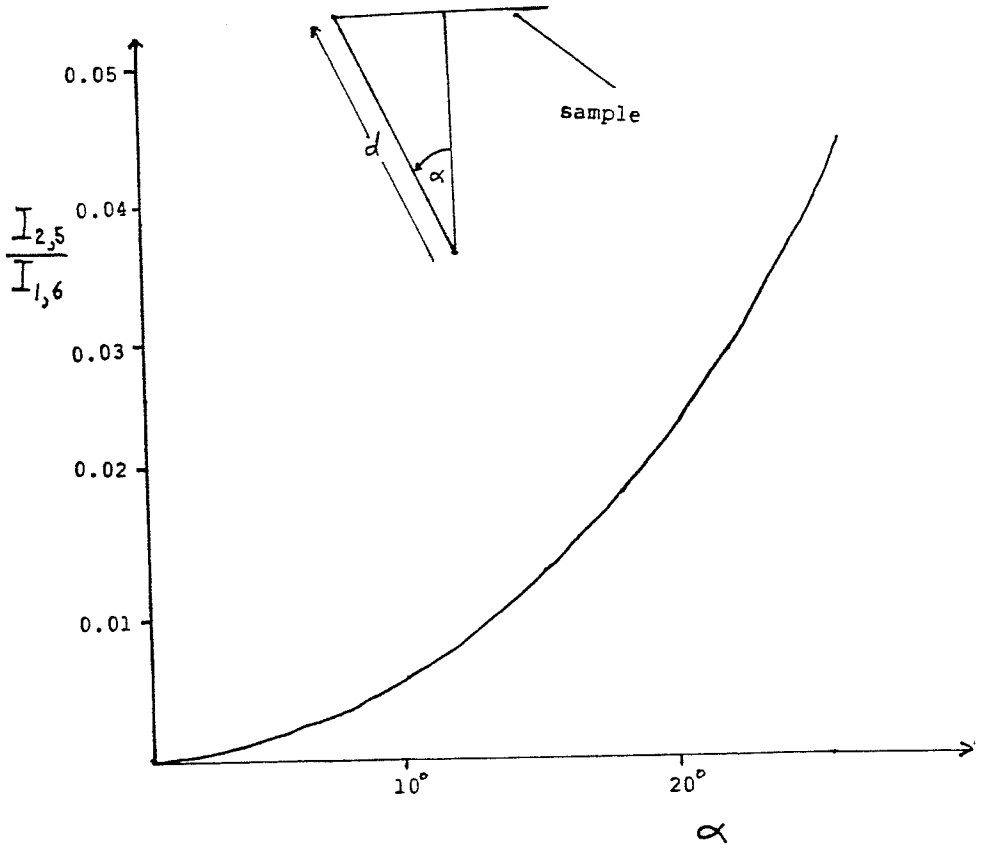

Fig a.1: Relative line intensities versus α for the case where $I_{2,5}$ =0 at α =0.

REFERENCES

J.J. Bara, B.F. Bogacz Mossbauer Effect Reference and Data J. 3 (1980) 154-163.

M. Carbucicchio Nuc. Instr. and Meth. 144 (1977) 225-229.

J. Chappert J de Physique Colloque C2,Supplement au No.3 40 (1979) p C2-107,C2-114.

A.G. Dirks, H.J. Leamy J. Appl. Phys. 49 (3) (1978) 1735-1737.

N.N. Greenwood and T.C. Gibb Chapman and Hall London 1971.

D. Henderson, M.H. Brodsky, P. Chaudhari App Phys Lett, 25 No. 11 (1974) 641-643.

D. Liljequist,B. Bodlund-Ringstrom Nuc. Instr. and Meth. 160 (1979) 131-136.

O.Massenet Nuc. Instr. and Meth. 153 (1978) 419-421.

P.J. Picone and A.H. Morrish J. Appl. Phys. 53 (1982) 2471-2476.

M.J. Tricker, L.A. Ash, T.E. Cranshaw Nuc. Instr. and Meth. 160 (1977) 307-309.

M.J. Tricker,L.A. Ash,and W. Jones Sur. Sc. 79 (1979) L333-336.

S. Tsunashima, T. Shinoda, H. Miyatake, S. Uchiyama J App. Phys. 51 (11) (1980) 5901-5905.

R. Wang and M.D. Merz Phys. Stat. Sol.(a) 39 (1977) 697-703.